Volume 1 | Number 1 | Jan 2013 | Pages 1–100

Nanoscale

www.rsc.org/nanoscale

ROYAL SOCIETY OF CHEMISTRY

ROYAL SOCIETY OF CHEMISTRY

www.rsc.org/nanoscale

Nanoscale

ARTICLE

Simple fabrication of three-dimensional porous polymer film as diffuser for organic light emitting diodes

Byung Wan Lim and Min Chul Suh[*]

We have investigated a simple and cost-effective fabrication method of porous polymer film employing spin-coating process during continuous supply of water droplets by ultrasonic humidifier. The resultant porous polymer film showed ~40% optical haze so that this film can be used as a diffuser film for strong microcavity OLEDs. Especially, we focused to control the surface morphology to give a three-dimensional (3D) multi-stacked nanocave structure because we already learned that the two-dimensional nanoporous structure gives serious loss of luminance in the front direction. As a result, we found that a 3D-ordered multi-stacked nanocave structure with a relatively small diameter and distribution range of 300–500 nm can be obtained by precise control of an elastic bouncing behaviour of supplied water droplets. From this approach, we found that the 3D nanoporous polymer film can effectively reduce the viewing angle dependency of strong microcavity OLEDs without any considerable decrease in the total intensity of the out-coupled light.

Introduction

Due to their unique properties, porous films have attracted a lot of scholarly attention. Among other applications, such films with two-dimensional (2D) or three-dimensional (3D) ordered structure can be used as membranes for bio-applications, catalysts for certain reactions, materials for nano-imprinting technology, and so on [1–11]. Most importantly, their unique pore structure with periodicity in the sub-micron size that can interact with visible light enables using them in optical applications.

The representative method to prepare such porous films is to use the thermocapillary convection behaviour of monodispersed hot water vapours supplied by a vaporizer on the cold surface of a polymer solution [12].

In other words, the water vapours (by a carrier gas such as nitrogen or air) condensed on the surface of the polymer solution make the spherical caves by sinking and drying (see Fig. 1). Interestingly, the shapes and sizes of the caves formed near the polymer surface are reasonably uniform (300–500 nm). Indeed, a large temperature difference between water vapours and the surface of the polymer solution will lead to thermocapillary convection and stabilize the condensing water droplets on or at the polymer solution surface [12]. A similar temperature gradient between the drops ensures stability and lack of coalescence between water droplets, which occurs closely packed hexagonal 2D ordered structure. Another method that does not involve thermocapillarity can only be carried out through an elastic bouncing of the water droplets near the surface of the polymer solution. In this scenario, the condensing

water droplets are kept them apart during mixing with the evaporating solvent, as it escapes from the surface, providing thus a separating layer between the two droplets. As long as the interaction time between the droplets is shorter than the time required for the vapour to escape the interstices, the two droplets will interact elastically, where the water droplets could maintain their forms without coalescence. In this case, closely packed hexagonal arrays cannot easily be obtained by the second method. Meanwhile, nanostructures can change optical properties of materials, such as optical dispersion, transmission, and reflection via scattering and interference. By engineering the degree of order in various dielectric nanostructures, one can control the light propagation, spontaneous emission, localization, lasing, and so on. However, the regular spatial self-organization of those nanostructured pores with hexagonal symmetry could cause an undesirable diffraction pattern from the film [13–21]. Thus, in this study, we prepared randomly dispersed porous polymer films with nanopores on the surface and inside polymer layers by simply using an ultrasonic humidifier as a water mist (or droplet) supplier. Said differently, the reduced thermocapillary convection motion and coalescence behaviour between water vapours due to a reduced temperature difference between the solution surface and water droplet could lead to smaller and randomly distributed nanopores on the polymer films. We applied those porous polymer films to the strong microcavity OLEDs to achieve the desired Lambertian-like distribution of emissions by optical scattering.
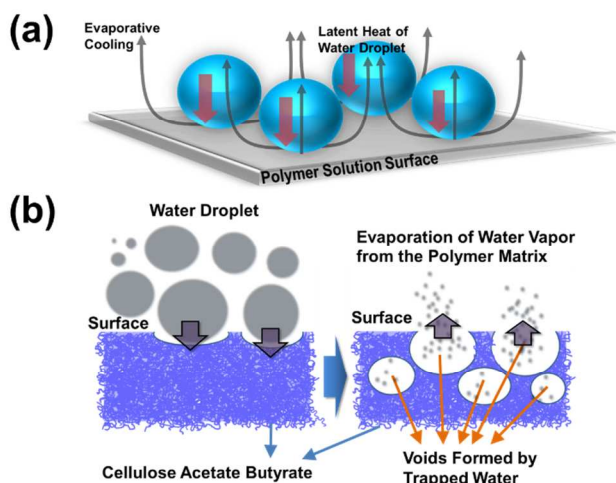

Fig. 1 The formation mechanisms of the porous film by (a) thermo capillary convection and (b) elastic bouncing.

Experimental Section

Polymer solution and porous polymer film

CAB (butyryl content: 35-39 %, M_w: 16,000 and 70,000 g/mol) was purchased from ACROS and used as a material for preparation of a diffuser layer. CAB solution with 8wt% of concentration was prepared in THF and chloroform to investigate a mechanism to form a porous CAB film (M_w: 16,000). To investigate a concentration effect, CAB (M_w: 70,000) solutions with three different concentrations (15, 8, and 3 wt %) were prepared in chloroform and dissolved by sonification for 10 min and vortex mixer for 10 min.

The solution was coated on the backside of glass substrate by using a spin-coating method. During the spin-coating process, the water mist was directly supplied to the spin-coater by ultrasonic type humidifier. The water mist was supplied consistently to maintain ~ 90% relative humidity (RH) condition. After spinning and evaporation of the solvent, the resultant glass substrate with CAB film was dried for 10 minutes at room temperature. After finishing the drying process, we investigated the morphology of polymer films with numbers of nanopores by using FE-SEM (HITACHI, S-4700) and AFM (Atomic Force Microscopy) technologies. The haze of porous polymer film on bare glass was measured using a NDH-5000 haze meter from Nippon Denshoku Industries.

OLEDs fabrication and characterization

Clean glass substrates precoated with ITO / Ag / ITO layers were used to investigate top-emission properties. Line patterns of anode materials were formed on glass by the photolithography process. A bank layer was also formed on the anode and glass substrate by the photolithography process to define the pixel aperture area by using photoresist. The glass substrates with the anode, as well as bank layer, were cleaned by sonification in an isopropyl alcohol and acetone, rinsed in deionized water, and, finally, irradiated in a UV-ozone chamber. All organic materials were deposited by the vacuum evaporation technique under the pressure of ~1x10⁻⁷ Torr. The deposition rate of the organic layers was about 1 Å/s. After deposition of all organic layers, Al (aluminium) was successively deposited without breaking vacuum at the deposition rate of 3 Å/s.

The current density-voltage (*J-V*) and luminance-voltage (*L-V*) data of the OLEDs were measured by Keithley SMU 238 and Minolta CS-100A, respectively. The electroluminescence (EL) spectra and the Commission Internationale De'Eclairage (CIE) coordi-

Nanoscale

nate were obtained using a Minolta CS-2000A spectro-radiometer. The OLED area was 4 mm^2 for all the samples used in this study. During the measurement of the integrated spectra for all the emission angles, an integrating cube (IC2, StellarNet. Inc.) was connected to the spectrometer.

Results and discussion

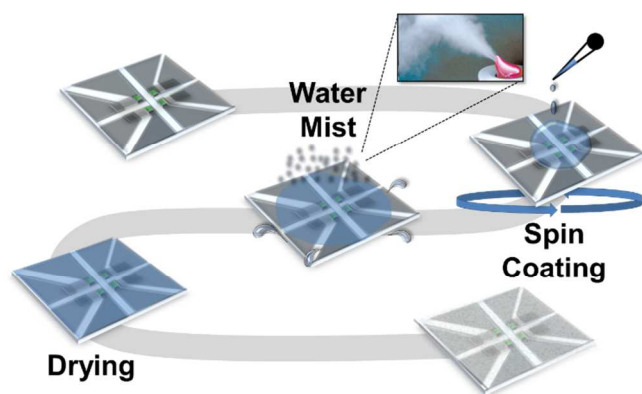### Preparation of 3D nanoporous polymer films

Fig. 2 Schematic illustration of 3D porous film formation on OLED device by humidifier method.

In a previous study, we prepared 2D porous polymer films through a simple spin-coating process with a continuous supply of water mist into the center of the chamber having a cylindrical body (23 cm in diameter and 17 cm in height) with a removable cover on a spin coater with the spinning chuck [22]. In other words, we supplied the water droplets to the spin coater simply by using an ultrasonic humidifier. However, we found that the 2D porous polymer film does not bring about a positive effect when it is used as a diffuser layer on a top-emission organic light emitting diode (OLED) with a strong microcavity. Indeed, plausibly due to a small light-scattering effect, it reduces the current efficiency of the devices due to a considerable loss of luminance towards the front direction without a significant improvement of viewing angle dependency.

Therefore, in order to enhance the light-scattering effect by optimization of the condition of the polymer solution (e.g. the molecular weight of the polymers, solvent, concentration, etc.), we need to change the surface morphology of films to 3D multi-stacked nanocave structures.

In principle, the thermal evaporation methods or vaporizer method (for generation of water vapour) have been extensively studied to prepare nanoporous polymer films [4-13]. However, these methods have been regarded as limited process to be applied to a mass production for flat panel displays. Thus, we need to investigate an alternative method. And we found that an ultrasonic humidifier method could be very simple to supply a water mist into the spin coating chamber. However, to date, there have been no extensive studies relating to an ultrasonic humidifier method. Thus, we investigated the basic behaviour of such method by comparing that of vaporizer method during formation of nanoporous film by varying the solvent, concentration of the polymer solution, spin coating rate, and so on.
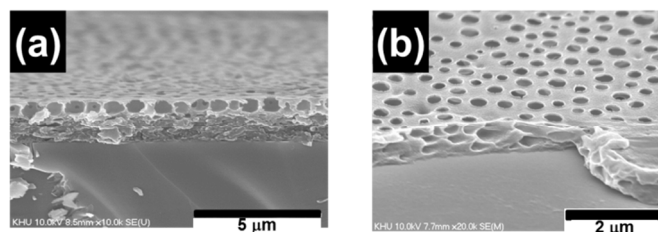

Fig. 3 SEM images of porous polymer films obtained from the different solvent condition. (a) THF; (b) chloroform.

Firstly, we investigated the solvent effect of polymer film process proceeded by ultrasonic humidifier method. To compare such method with well-known vaporizer process, we used same condition as that used in the previous report [8]. Fig 3a shows the SEM image of cross section of spin-coated CAB film (M_w: 16,000) obtained from THF solution (8 wt %, from spinning rate of 1,000 rpm). Film morphology prepared by pure THF solution of CAB showed randomly dispersed nanoporous structure formed only at the top surface. This is very similar to that obtained by M. S. Park except that the film obtained from the vaporizer method gives closely packed pores [8]. In contrast, the closely packed pores hardly occur from the ultrasonic humidifier method because the mixing of droplets with the solution is dominant over the coalescence of water vapour because such method uses the previously condensed water droplets. However, in both cases, condensed water droplets sink into the solution, are depleted by the mixing with the water-miscible solution. Thus, only 2D structure could be obtained from the pure THF solution by both methods.

On the other hand, we could obtain a multi-stacked nanocave structure (3D structure) from humidifier method as shown in Fig 3b, when we utilize a water immiscible chloroform solution of CAB. This is attributed to the fact that the nucleation rate of water condensation (from vaporizer method) was greatly reduced. Besides, spin coating process significantly suppresses coalescence between water droplets because solvent evaporates much faster than coalescence. Hence,

the ultrasonic humidifier method which is the way to use a previously condensed water droplets is more effective to make 3D multi-stacked nanocave structure from such solution because the mixing of condensed water and water-immiscible solvent inside the film is much more efficient.
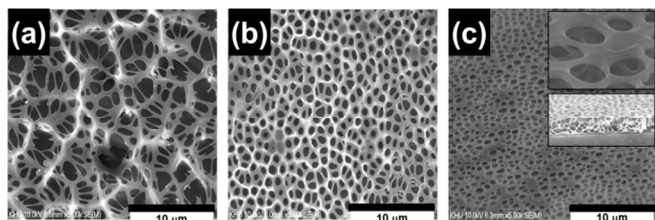

Fig. 4 SEM images of porous films formed with different CAB concentrations of (a) 15wt%; (b) 8wt%; (c) 3wt%.

Secondly, we investigated the concentration effect of polymer film process prepared from various polymer solutions with different concentrations of CAB. For this experiment, we used CAB with higher molecular weight (M_w: 70,000) to obtain thicker porous film to enhance the diffuser property. As a result, each polymer solution with a different concentration yielded an entirely different morphology (see Fig. 4). Fig. 4 shows SEM images of the top surface of the CAB film prepared by spin-coating of three different polymer concentrations (15, 8, and 3 wt %) in chloroform from spinning rate of 1,000 rpm. Very interestingly, the malformed morphology was obtained when the concentration of the polymer solution was very high (15 wt %, see Fig. 4a). This means that the high surface tension of the thick polymer solution may inhibit the water droplets from sinking or mixing into the polymer solution during spin-coating. Said differently, while, at a higher polymer concentration, inlets of consecutive condensed water is required to form multi-stacked water droplet morphology, the ability to stabilize droplets in the polymer solution in such condition is greatly reduced due to a slow evaporation of waters and solvents inside the highly viscous polymer solution. On the other hand, at a lower concentration, fast evaporation (and solidification) of water droplets mixed with the polymer solution could be possible to give better morphology as shown in Fig. 4b. In the same manner, the malformed morphology was successfully diminished and finally yielded an ordered form. As a result, a relatively ordered structure was obtainable from the thin polymer film with a concentration of ~3 wt % (see Fig. 4c). From the oblique view of the polymer surface, we could observe that the resultant film had the multi-stacked nanocave structure mentioned above (see inset of Fig. 4c). In addition,

while the sizes of the first layers of porous structures were almost identical, the sizes of the second or inside layers of the pores became smaller when the pores were formed in the inner part of the polymer film. Nevertheless, they could be used as an optical application because they still have nanosize morphology.

Thirdly, we investigated the spin coating rate dependence of polymer film prepared from different spinning rate (1,000 – 3,000 rpm). As shown in Fig. 5, the pore density on the surface decreased as spinning rate increased. This means that a sinking or a mixing of the water droplets into the polymer solution becomes difficult if the spinning rate is too high. Said differently, inlets of consecutive condensed water are limited at the high spin speed so that the formation of multi-stacked morphology is greatly reduced.
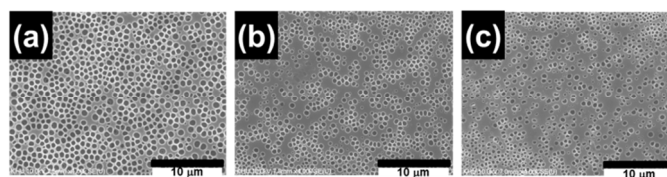

Fig. 5 SEM images of porous films formed by different spinning rates; (a) 1,000 rpm; (b) 2,000 rpm; (c) 3,000 rpm.

Optical properties of 3D porous polymer films

Porous polymer films formed on the surfaces of substrate by a simple spin-coating process in the highly humid atmosphere were investigated by atomic force microscopy (AFM; see Fig. 6). The dark areas in Fig. 6 are pores created by continuous interaction of polymer solution with supplied water mists (or droplets). The pores are small but evenly distributed (see Fig. 6a). However, they can be utilized as an optical diffuser layer because they still have nanosize morphology as mentioned above, which are desirable to interact with visible light because the pore sizes in this film are comparable to the wavelength of the visible light. From this view point, we could use those films as a diffuser layer to re-distribute the frontally directed visible light from the OLED with strong microcavity structure [23–26]. AFM measurements verified that nanopores with a diameter and distribution range of 300–500 nm were acquired. The inset images of Fig. 6a are the fast Fourier transforms (FFTs) of the formed nanopores and the FFTs resulted in faintly symmetrical rings. This means that the nanopore arrays have a range of diameters with randomly dispersed orientations. As a result, the diameters of the pores and the obtained distances were

supposed to occur at a significant scattering in the visible light region without a serious diffraction pattern of the light to a certain direction. The pore depths were in the 300–500 nm range, i.e. appropriate for efficient scattering in the visible light region. The transmittance haze is defined as the ratio of the diffused light to the total transmitted light. Scattering media usually increase the optical haze, as the light scatters in all directions.
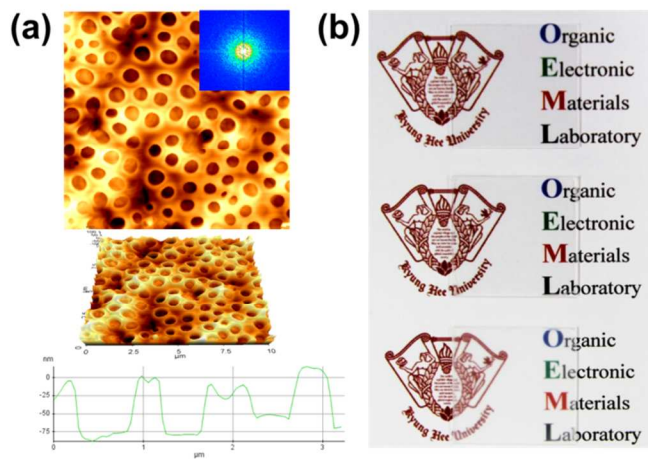

Fig. 6 (a) AFM images of the porous film (top: nanopores on surface, inset: fast Fourier transforms of the porous film, middle: 3D-oblique view of porous film with $100\mu m^2$ dimensions, bottom: depth profile of the film surface); (b) Photographic images for comparison of haze (top: bare glass, middle: film without nanopores, bottom: porous film).

In display applications, the increased haze may blur the pixel and ruin the resolution of the devices. While the haze value of the porous polymer film was measured as 40%, the haze of a glass without nanopores was ~0%. For comparison of the haze, images of the bare glass i.e. the glass with the CAB film without and with nanopores are shown in Fig. 6b. Although the characters under the glass substrate coated with porous polymer film are blurred, no significant difference in clarity between the bare glass and the randomly dispersed porous film coated on the bare glass was observed because the transmittance of the nanoporous film is still very high (~ 94%).

Device characteristics of 3D porous polymer films as a diffuser layer for OLED with strong microcavity structure

To evaluate the performance of a randomly distributed porous polymer film created by a simple coating process as a diffuser layer, highly efficient green phosphorescent OLEDs (PHOLEDs) were

fabricated. To prepare PHOLEDs, we used indium tin oxide (ITO) / silver (Ag) / ITO as an anode, *N,N'*-bis (naphthalen-1-yl)-*N,N'*-bis(phenyl)benzidine (α-NPB) as a hole transport layer; 1,4,5,8,9,11-hexaazatriphenylene hexacarbonitrile (HA T-CN) as an intrinsic *n*-type material to improve the hole transporting ability of α-NPB; 4,4',4"-tris(carbazol-9-yl)triphenylamine (TCTA) as an exciton blocking layer; beryllium bis(2-(2'-hydroxyphenyl) pyridine (Bepp₂) and bis(2-phenyl-pyridine)(acetylacetonato)iridium(III) [Ir(ppy)₂(acac)] as host and dopant materials for an emission layer; 4,7-diphenyl-1,10-phenanthroline (Bph en) as an electron transport layer and a hole blocking layer; lithium fluoride (LiF) as an electron injection layer (EIL); and aluminum (Al) as a cathode. The structure of green PHOLED and the energy diagram of the materials used are shown in Fig. 7a-b.
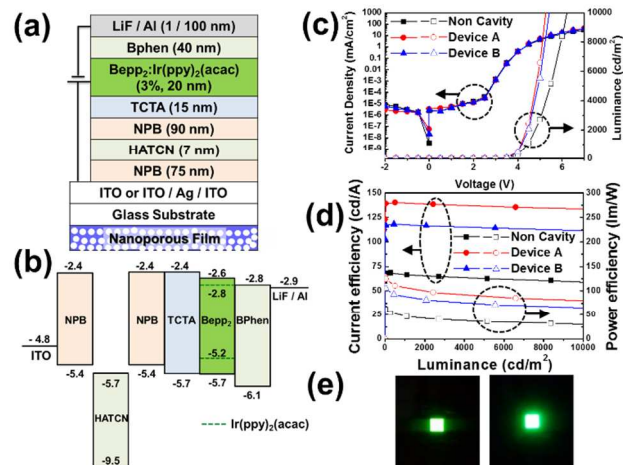

Fig. 7 (a) noncavity and/or cavity OLED device structures in this study; (b) energy band diagram of the device; device characteristics of microcavity OLEDs without a porous film (Device A), with porous film (Device B) and non-cavity OLED (a) current density (*J*) - voltage (*V*) characteristics (solid symbol) and luminance (*L*) - voltage (*V*) (open symbol) characteristics; (d) current efficiency-luminance characteristics (solid symbol) and power efficiency-luminance characteristics (open symbol); (e) the electroluminescent images of the devices without/with porous film (left/ right).

The detailed configuration of OLEDs prepared for this study was ITO (7 nm) / Ag (18 nm) / ITO (7 nm) / NPB (75 nm) /HAT-CN (7 nm) / NPB (90 nm) / TCTA (15 nm) / Bepp₂ : Ir(ppy)₂(acac) (3%, 20 nm) / Bphen (40 nm) / LiF (1.5 nm) / Al (100 nm). We used 2nd-order microcavity condition with a thick HTL thick to prevent leakage currents, as the total thickness of the 1st-order cavity device is too thin to cover the dust

particles plausibly originating from the anode side [27-28]. The resultant green PHOLEDs fabricated with this device configuration were labeled to Device A, Device B, and Non-Cavity Device, respectively. The specifications are as follows: Non-Cavity Device: The green PHOLED on the transparent anode (ITO); Device A: The green PHOLED on the semitransparent anode (ITO / Ag / ITO) without diffuser layer; Device B: The green PHOLED on the semitransparent anode (ITO / Ag / ITO) with diffuser layer. Fig. 7c shows the current density–voltage (*J–V*) and luminance–voltage (*L–V*) characteristics of fabricated green PHOLEDs. At a given constant voltage of 5V, current density values of 4.20, 4.86 and 4.86 mA/cm^2 were observed from Non-Cavity Device, Device A, and Device B, respectively. The driving voltages to reach 1,000 cd/m^2 were 4.43, 4.12, and 4.18 V for the Non-Cavity Device, Device A, and Device B, respectively. Indeed, at a given constant luminance of 1,000 cd/m^2, the current and power efficiencies were 66.9 cd/A and 50.9 lm/W for the Non-Cavity Device, 139.8 cd/A and 114.1 lm/W for Device A, and 117.8 cd/A and 95.1 lm/W for Device B, respectively (see Fig. 7d). Unfortunately, the current efficiency at 1,000 cd/m^2, which is associated with a frontally directed emission, decreased by 15.7 % when we added the diffuser layer due to its high haze value (~ 40%). Meanwhile, the maximum current and power efficiencies were 68.5 cd/A and 63.1 lm/W for the Non-Cavity Device, 140.3 cd/A and 128.9 lm/W for Device A, and 118.3 cd/A and 108.0 lm/W for Device B, respectively.

Table 1 Summary of device characteristics of OLEDs

Items	Non-Cavity Device	Device A	Device B
Turn-on voltage [a]	3.0 V	3.0 V	3.0 V
Operating voltage [b]	4.4 V	4.1 V	4.2 V
Efficiency [b]	66.9 cd/A 50.9 lm/W	139.8 cd/A 114.1 lm/W	117.8 cd/A 95.1 lm/W
Efficiency [c]	68.5 cd/A 63.1 lm/W	140.3 cd/A 128.9 lm/W	118.3 cd/A 108.0 lm/W
EQE [d]	17.5%	27.1%	26.9%
(x, y) [e]	0.333, 0.617	0.259, 0.705	0.240, 0.708
(u', v') [f]	0.137, 0.570	0.094, 0.580	0.087, 0.578

[a] Measured at 1 cd/m^2. [b] Measured at 1,000 cd/m^2. [c] The efficiency values at the maximum point. [d] Measured from the integrating sphere method. [e] Colour Coordinate by CIE (1931) system. [f] Colour coordinate by CIE(1976) system.

As a result, the total enhancement of the out-coupled emission by the microcavity effect combined with the diffuser layer was reached only about 76% (cf. enhancement merely by microcavity effect: ~109%). Incidentally, Device B looks more diffusive, that is, light hardly is emitted frontally which is more desirable, as shown in Fig. 7e. In other words, we found that the

nanoporous CAB film fabricated by proposed humidifier method could be utilized as a diffuser film. To more rigorously investigate about this phenomenon, we measured the total flux of light emission by integrating sphere and obtained similar EQE (External Quantum Efficiency) values of 27.1 and 26.9 % for Device A and B, respectively (see Fig. 8a). Both values are significantly increased compared to that of Non-Cavity Device (EQE: 17.5%) which means that the diffuser film only spread the direction of the emission laterally (see Fig. 8b) without any considerable loss of the total light emission. As a result, we obtained a somewhat wider light distribution from Device B (see Fig. 8b).
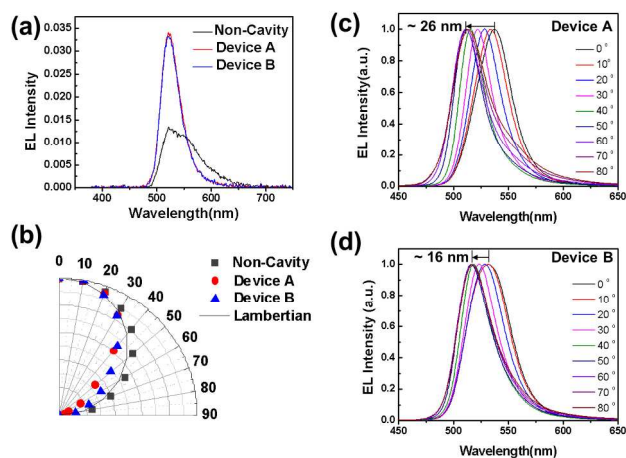

Fig. 8 (a) Electroluminescence(EL) spectra of the fabricated OLEDs measured by an integrating sphere; (b) polar plot of normalized EL intensities varying with the viewing angle of fabricated devices; normalized electroluminescence spectra varying with the viewing angle of (c) Device A; and (d) Device B.

To identify diffusive behaviour of the porous film accurately, we measured the EL spectra of each device with varying the viewing angle and the results are shown in Fig. 8c-d. Interestingly, as the TOLED without the diffuser film showed a serious hypsochromic shift [λ_{max}: 537 nm (0°) → 511 nm (80°), 26 nm], while the TOLED with diffuser (haze: 30%) showed much less viewing angle dependency [λ_{max}: 532 nm (0°) → 516 nm (80°), 16 nm]. As the viewing angles increased from 0° to 80° off the surface, a significant hypsochromic shift of Device A is mainly due to the strong microcavity effects originating from the phase change upon the variation of the viewing angle following the general formula shown below [29-34]:

$$\lambda(\theta) = 4\pi(\Sigma n_i d_i)\cos(\theta)/(\phi(\theta)\text{-}2\pi m) \qquad (1)$$

where, $\Sigma n_i d_i$ is the cavity length; n_i and d_i are the refractive index and thickness of the i-th organic layer; $\phi(\theta)$ is the total phase shift caused by reflections at two electrodes; and m is the cavity mode number. In this study, we utilized $m = 1$. Generally, $\lambda(\theta)$ blue shifts with increasing viewing angle due to a cosine dependence on viewing angle (θ). In order to reduce the change of $\lambda(\theta)$ with viewing angle (θ), one can counter-increase the cavity thickness with viewing angle (θ) and increases n_i with reducing λ. Otherwise, we could reduce such dependence by using diffuser film. As a result, while Device A showed a larger color coordinate [CIE (1931)] change from (0.259, 0.705) to (0.216, 0.655) when the viewing angle increased from 0º to 80º, Device B showed a relatively small color change from (0.240, 0.708) to (0.213, 0.688). This is a very promising result, although the emission pattern of the strong cavity bottom emission OLED (Device B) with diffuser layer still deviated from the desirable Lambertian distribution in the polar plot (see Fig. 8b). The trend of such reduced viewing angle dependency after the introduction of the diffuser film is very similar to that previously reported in Liu et al. [35].

Conclusion

We obtained porous polymer film with a ~40% optical haze as a diffuser. It was fabricated by a simple spin-coating process during continuous water mist supply by humidifier. The pores were created by an elastic bouncing mechanism (rather than thermo-capillary convection mechanism) of the supplied water droplets. The shapes and sizes of the caves formed near the polymer surface are randomly distributed with the relatively narrow pore sizes distribution (300–500 nm). We applied such porous polymer film to microcavity OLEDs to investigate the possibility to use it as a diffuser layer. The resultant porous polymer film effectively reduced the viewing angle dependency of microcavity OLEDs although it occurred some pixel blurring phenomenon. Despite its negative effect on efficiency drop towards the front direction and pixel blurring, the introduction of porous polymer films as scattering media on the back side of the glass substrate eliminated the viewing angle dependency. Thus, this approach is a promising method to overcome the serious drawbacks of microcavity OLEDs, such as a considerable viewing angle dependency.

Acknowledgements

Department of Information Display and Advanced Display Research Center, Kyung Hee University
Seoul 130-701, Republic of Korea
E-mail: mcsuh@khu.ac.kr

Notes and references

1 N. R. Cameron, *Polymer,* 2005, **46**, 1439–1449.
2 P. H. Pfromm, I. Pinnau, W. J. Koros, *J. Appl. Polym. Sci*., 1993, **48**, 2161–2171.
3 R. R. Li, P. D. Dapkus, M. E. Thompson, W. G. Jeong, C. Harrison, P. M. Chaikin, R. A. Register, D. H. Adamson, *Appl. Phys. Lett*. 2000, **76**, 1689–1691.
4 M. S. Park, Y. Lee, J. K. Kim, *Chem. Mater.* 2005, **17**, 3944–3950.
5 O. Karthaus, N. Maruyama, X. Cieren, H. Hasegawa, T. Hashimoto, M. Shimomura, *Langmuir 2000,* **16***, 6071–6076.
6 T. Nishikawa, R. Ookura, J. Nishida, K. Arai, J. Hayashi, N. Kurono, T. Sawadaishi, M. Hara, M. Shimomura, *Langmuir* 2002, **18**, 5734–5740.
7 H. Yabu, M. Tanaka, K. Ijiro, M. Shimomura, *Langmuir* 2003, **19**, 6297–6300.
8 M. S. Park, W. Joo, J. K. Kim, *Langmuir* 2006, **22***, 4594–4598.
9 M. S. Park, J. K. Kim, *Langmuir* 2004, **20***, 5347–5352.
10 M. S. Park, J. K. Kim, *Langmuir* 2005, **21***, 11404–11408.
11 A. Bolognesi, C. Mercogliano, S. Yunus, M. Civardi, D. Comoretto, A. Turturro, *Langmuir* 2005, **21***, 3480–3485.
12 M. Srinivasarao, D. Collings, A. Philips, S. Patel, *Science* 2001, **292**, 79–83.
13 B. Francois, O. Pitois, J. Francois, *Adv. Mater.* 1995, **7**, 1041–1044.
14 J. Peng, Y. Han, Y. Yang, B. Li, *Polymer* 2004, **45**, 447–452.
15 G. Widawski, M. Rawiso, B. Francois, *Nature* 1994, **369**, 387–389.
16 O. Pitois, B. Francois, *Eur. Phys. J. B* 1999, **8**, 225–231.
17 O. D. Velev, T. A. Jede, R. F. Lobo, A. M. Lenhoff, *Nature* 1997, **389**, 447–448.

18 B, Gates, Y. Yin, Y. Xia, *Chem. Mater.* 1999, **11**, 2827–2836.

19 Z. Li, W. Zhao, Y. Liu, M. H. Rafailovich, J. Sokolov, *J. Am. Chem. Soc.* 1996, **118**, 10892–10893.

20 M. Park, C. Harrison, P. M. Chaikin, R. A. Register, D. H. Adamson, *Science* 1997, **276**, 1401–1404.

21 S. A. Jenekhe, X. L. Chen, *Science* 1999, **283**, 372–375.

22 B. W. Lim, H. S. Jeon, M. C. Suh, *Synth. Met.* 2014, **189**, 57–62.

23 Y. R. Do, Y. C. Kim, Y. W. Song, C. O. Cho, H. Jeon, Y. J. Lee, S. H. Kim, Y. H. Lee, *Adv. Mater.* 2003, **15**, 1214–1218.

24 J. M. Lupton, B. J. Matterson, I. D. W. Samuel, M. J. Jory, W. L. Barnes, *Appl. Phys. Lett.* 2000, *77*, 3340–3342.

25 M. Boroditsky, T. F. Krauss, R. Coccioli, R. Vrijen, R. Bhat, E. Yablonovitch, *Appl. Phys. Lett.* 1999, **75**, 1036–1038.

26 J. D. Joannopoulos, P. R. Villeneuve, S. Fan, *Nature* 1997, **386**, 143-149.

27 H. Y. Shin, M. C. Suh, *Org. Electron.* 2014, **15**, 2932-2941.

28 S. J. Cha, J. H. Jeon, M. C. Suh, *Org. Electron.* 2014, **15**, 2830-2836.

29 C. Lee, J. J. Kim, *Small* 2013, **22**, 3858-3863.

30 Y.-F. Liu, J. Feng, D. Yin, H.-F. Cui, X.-L. Zhang, Y.-G. Bi, D.-D. Zhang, L.-S. Liu, A.-W. Li, J.-F.Song, Q.-D. Chen, H.-B. Sun, *Org. Electron.* 2013, **14**, 1597–1601.

31 C.-H. Chang, H.-C. Cheng, Y.-J. Lu, K.-C. Tien, H.-W. Lin, C.-L. Lin, C.-J. Yang, C.-C. Wu, *Org. Electron.* 2010, **11**, 247–254.

32 C. Y. Ho, C. H. Choy, *Opt. Express.* 2007, **15**, 13288–13294.

33 S. M. Jeong, Y. Takanishi, K. Ishikawa, S. Nishimura, G. Suzaki, H. Takezoe, *Opt. Commun.* 2007, **273**, 167–172.

34 C. L. Lin, H. C. Chang, K. C. Tien, C. C. Wu, *Appl. Phys. Lett.* 2007, **90**, 071111.

35 C. C. Liu, S. H. Liu, K. C. Tien, M. H. Hsu, H. W. Chang, *Appl. Phys. Lett.* 2009, **94**, 103302.

Nanoscale Accepted Manuscript